Evaluation of Ozone Generation in Volume Spiral-Tubular Dielectric Barrier Discharge Source

Pawel Zylka [ID]

Department of Electrical Engineering Fundamentals, Wroclaw University of Science and Technology, Wyb. Wyspianskiego 27, 50-370 Wroclaw, Poland; pawel.zylka@pwr.edu.pl

Abstract: Ozone, due to its high reactivity cannot be stockpiled, and thus requires to be generated on-demand. The paper reports on laboratory studies of O_3 generation in a volume dielectric barrier discharge (DBD) tubular flow-through system with a coaxial-spiral electrode arrangement. Its performance is experimentally verified and compared to a commercial surface DBD O_3 source fitted with a three-electrode floating supply arrangement. The presented volume DBD design is capable of steadily producing up to 4180 ppm_v O_3 at 1 Nl/min unprocessed atmospheric air intake and 10 kV 1.6 kHz sinusoidal high voltage supply corresponding to 67 g/kWh O_3 production yield increasing to 93 g/kWh at 100 Nl/min air intake. The effects of high voltage supply tuning are also investigated and discussed together with finite element method simulation results.

Keywords: ozone; temperature; destruction; dielectric barrier discharge; surface discharge

1. Introduction

Ozone has been recently extensively applied as a potent oxidizing agent in many fields of science, technology and everyday life including chemical synthesis, semiconductor surface treatment, water disinfection, destruction of pollutants and odor removal, purification of products, decolorization (bleaching), vermin and insects control, automotive fuel afterburning, skin treatment and dental care, just to name a few [1–4]. However, at the same time, ozone is considered a highly toxic gas—its PEL (Permissible Exposure Limit) and REL (Recommended EL) health limits are as low as 0.1 ppm (0.2 mg/m^3) while IDLH (Immediate Danger Lethal Dose) is set at 5 ppm [5]. Lowest lethal concentrations (LCLo) range from 4.8 ppm in rats (for 4 h exposure) to 50 ppm in humans (for 30 min contact) [6]. Ozone (discovered by F. Schoenbein in 1839) is a colorless or, at higher concentrations, pale blue gas containing three oxygen atoms in its molecule (O_3), thus it is a triatomic allotrope of O_2. It is highly unstable and readily reacts with other substances as a powerful oxidizer. In some references, it is regarded as odorless although other sources quote it as having "very pungent odor" or even "characteristic, pleasant odor" [6] (however, such inconsistency is rather related to secondary smell sensation caused by malodorous products of olfactory tissue oxidized by O_3 than its primary olfaction). O_3 is generated naturally in the Earth stratosphere by photolysis of molecular O_2 by short-wave (λ < 200 nm) solar ultraviolet (UV) radiation, which produces excited oxygen O* atoms, undergoing binding collisions with O_2 to form O_3 molecules afterward.

O_3 is also readily produced (in so-called three-body reaction, involving O, O_2 and O_3) in electrical discharges generated in pure oxygen or in atmospheric air and such processes are commonly applied in laboratory and industrial ozone generators. Such systems commonly make use of non-thermal plasma generated in dielectric barrier discharges (DBD), corona or surface discharges as it allows to attain elevated effectiveness of O_3 generation process and to perform it on-demand and on-site, directly when and where ozone is required as it essentially cannot be effectively stockpiled [7].

Corona discharge (also referred to as pre-discharge) arises when the dielectric strength of a discharge gap is exceeded only locally in a strongly non-uniform electric field resulting in a situation when a discharge channel cannot develop into a spark or flashover discharge. It appears as a dim filamentary discharge emanating outward from the high voltage electrode of a small curvature radius. Corona discharge term is commonly used to describe discharges developing between gas-insulated bare metal electrodes without a solid dielectric involved however, some authors use this term in conjunction or even interchangeably with DBD [8]. Corona discharges exist in several forms depending on the electrode geometry and supply voltage type and polarity, including intermittent, glow, burst, pulse, pulseless, streamer and leader corona. Corona discharge may be generated using either DC or AC voltage although both types of pre-discharge differ in character. The term surface corona discharge (or creeping discharge) is used in a situation when the electrode configuration results in an electric field with a substantial tangential gas–solid interphase component and thus the corona discharges propagate (slide) along the interphase. A comprehensive study of topics related to corona discharge and its use in O_3 making may be found in the relevant literature [8–10].

On the other hand, DBD (named also as silent discharge or ozonizer discharge) is also a non-thermal electrical discharge developing in a gas phase except that a layered barrier insulation system containing solid dielectric(s) is involved. In such configuration, a uniform (or slightly non-uniform) electric field is strong enough to produce a localized breakdown in the entire gas gap but not in the dielectric barrier. As such an arrangement can only pass the displacement current, DBDs are generated using AC electric supply. Volume DBD is in some way analogous to cavity discharge (internal partial discharge, PD) developing in a gaseous void inside a solid dielectric subjected to AC high voltage stress. To illustrate this analogy, a bird's eye view photographs of the spatial distribution of DBD developing in a lens-like air gap formed in a polymeric body at various AC supply voltages are presented in Figure 1. In such an exotic gas cavity, taken after gas hollows present in voided ferroelectric material, DBD starts developing mostly near the rim of the void and tends to shift towards the void's center as the voltage is ramped up [11].
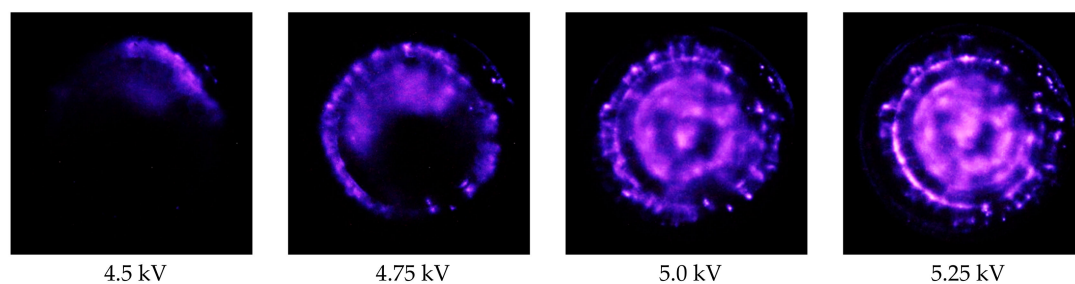

| 4.5 kV | 4.75 kV | 5.0 kV | 5.25 kV |

Figure 1. Spatial distribution of DBD developing in a lens-like 1.1 mm high and 16 mm in diameter air gap formed in 2.1 mm thick polyethylene terephthalate polyethylene terephthalate (PET) body at various 100 Hz AC supply voltages (peak value).

Volume DBD at atmospheric pressure consists of a large number (ca. $10^6/cm^2$ s) of randomly appearing but spatially-localized short-lived (ca. 100 ns) microdischarges. They take the form of thin (ca. 100 μm wide) cylindrical columns (filaments) normal to the gas-dielectric interphase and developing into much larger footings at the dielectric exterior while individual columns are separated by a non-plasma gaseous medium. The microdischarge activity results in short (a few ns), high-frequency current pulse trains registered in the discharge circuit during each AC voltage raise period. In the filament mode, observed at elevated (atmospheric-like) pressure in most gases (including air) each weakly ionized microdischarge channel is formed by a fully-developed but transient glow discharge dissipating just microjoules of energy. Volume DBD channels contain thus non-thermal non-equilibrium plasma. Consequently, thermal effects of volume DBD related to gaseous medium heating are minute (typically below 10 °C is observed in the air in mm-range discharge gaps). The spatial and temporal DBD parameters depend on the supply power density while the strength of DBD

is mainly determined by discharge gap width, gas properties (composition, pressure, humidity and flow rate) and dielectric barrier properties. Similarly to surface corona discharges, stable surface DBD (SDBD) may also be initiated over a dielectric surface using a tangential electric field shaped by a system of electrodes in creepage configuration located on opposite walls of a dielectric barrier. The electrodes may be partially or completely embedded in the dielectric or a three-electrode variation of such set-up may be used, which involves additional capacitively coupled floating-potential surface electrode. A detailed and comprehensive discussion of the DBD and SDBD physics, plasma chemistry, developments and applications may be found in the relevant literature [12–16].

Application of volume DBD for ozone production has been well-known for over a century as it was introduced by W. von Siemens already in 1857 in his air/oxygen-fed AC-energized ozone generator [17]. The original design consisted of two coaxial glass pipes forming a narrow annular gas flow channel in which silent discharges were sustained using alternating electric field formed by two electrodes located also coaxially but outside the discharge channel. Figure 2a briefly illustrates various flat and concentric electrode–barrier–gap configurations, commonly used in volume DBD while Figure 2b schematically outlines conventional SDBD electrode–barrier arrangements (including 2- and 3-electrode as well as uncovered and buried electrode designs).
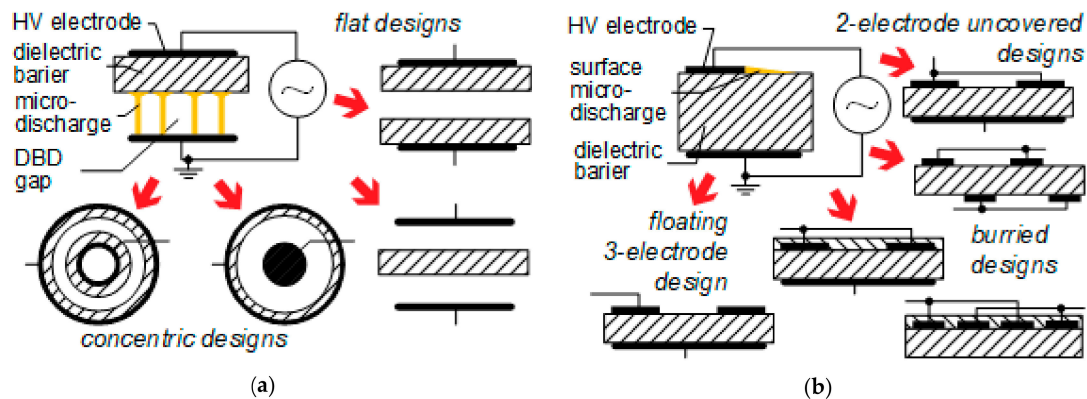

Figure 2. Schematic representation of various DBD electrode-barrier arrangement:(**a**) volume DBD, (**b**) surface DBD (drawings not to scale).

A growing environmental awareness of air pollution originated from fuel combustion exhausts (of either internal combustion engines or gas burners) has resulted in research aiming at fuel-burning performance improvement relying on combustion promotion attained by means of plasma/ozone processing of the intake air [18–20]. The latter may be realized in an automotive application using by-pass scheme DBD (exemplified in Figure 3) however it requires effective yet energy- and space-constrained air-fed non-thermal plasma and ozone generator. Thus, experimental verification of the electrical and thermal performance of a newly-designed volume DBD flow-through ozone generator (OG) of a spiral-tubular electrode design was presented in relation to a conventional volume cylindrical DBD as well as a commercial OG making use of SDBD generated in a floating electrode arrangement (advertised by its supplier as having amazingly high 8 g/h O_3 production). Improvement of O_3 generation effectiveness through high voltage (HV) electrical supply tuning was also investigated and discussed.

(**a**)   (**b**)

Figure 3. Hardware approach to process automotive engine intake air using manifold by-pass and non-thermal plasma/ozone generated in: (**a**) volume DBD, (**b**) SDBD.

2. Materials and Methods

A volume DBD OG of a tubular design, shown in Figure 4a, consisted of a metallic inner HV rod electrode (⌀18x250 mm) enclosed inside a silica (SiO_2) glass tube (⌀20/⌀25 mm) providing a 1 mm wide flow-through tubular gas channel, connected to gas ports, installed at end caps of the tube (as detailed in Figure 1a upper inset). The inner rod electrode was made either of brass (EN-CW617N grade) or duralumin (EN-2017 grade); in the latter case, its surface was covered with anodic-deposited Al_2O_3 layer. The silica glass tube was fitted with a grounded (GND) electrode made of Sn-platted thin Cu foil with a conductive adhesive layer (1183, 3M). It was firmly affixed to the silica tube external wall leaving no air bubbles at the $Cu-SiO_2$ interphase. Foil electrodes of a cylindrical as well a spiral design (as detailed in Figure 4a) were investigated; in each case 20 mm clearance between the foil electrode and the HV electrode metallic end caps ensured no surface sliding discharges in this area. The volume DBD OG was operated in a horizontal position with no forced cooling.
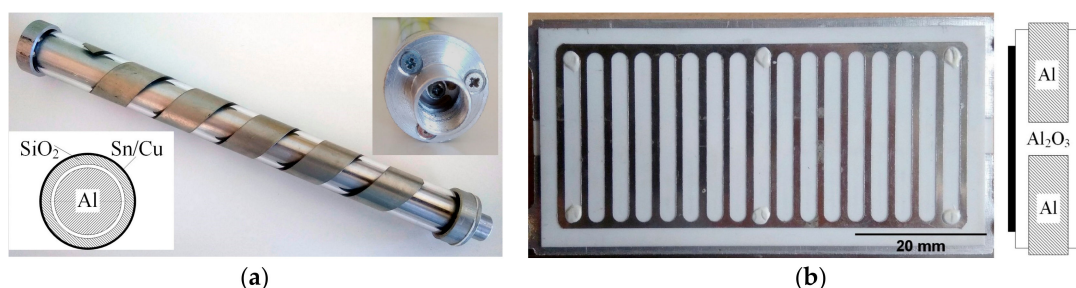

(**a**)   (**b**)

Figure 4. DBD OGs: (**a**) volume flow-through arrangement of a spiral-tubular design, (**b**) surface three-electrode metal-ceramic plate - a real view and schematic cross-section (drawings not to scale).

A commercial surface DBD OG (Sihon Ozone, China), used for comparative study, was claimed by its manufacturer to produce 8.0 g/h O_3 thanks to intensive surface DBDs generated in floating three-electrode arrangement. Metal-ceramic OG, shown in Figure 4b, consisted of two 1.3 mm thick duralumin (of unknown make) electrodes spaced by 5 mm and embedded in 2.8 mm thick alumina body forming 106x54x2.8 mm OG composite plate. The OG plate was fitted at both alumina faces with two 0.2 mm thick stainless steel, unprotected slotted electrodes (as drafted in the schematic cross-section shown in Figure 4b). Laboratory tests were conducted using two such SDBD OG plates collocated one over another, spaced vertically by 10 mm and placed in a hermetic metal vessel fitted with gas and electric supply ports.

Both tested OGs were supplied with unprocessed (not dehumidified) atmospheric laboratory air at 23–25 °C and 42%–45% RH (exemplifying commonplace laboratory conditions). The airflow rate was controlled using either a mass flow controller (F-201-CV, Bronkhorst) or a flow meter (SD6000, IFM Electronik), depending on the operational airflow rate. In low flow rate experiments (1.0 Nl/min)

the entire gas stream was passed through the O_3 analyzer while at moderate flow rates (10–100 Nl/min) the air-O_3 output stream was sampled at 1.0 Nl/min (as required by the O_3 analyzer).

O_3 concentration was monitored using a photometric analyzer at 254 nm UV radiation (BMT964, BMT Messtechnik), it was thus insensitive to N_2, H_2O or NO_x. O_3 volumetric concentration was expressed in ppm_v and all data (including flow rates expressed in Nl/min) was corrected for normal 1 atm and 0 °C conditions (expressing O_3 concentration in volumetric (ppm_v)=0.0001 (%v/v) is unambiguous and it does not require information on the carrier gas density as in case of (%wt/wt) [21]. The temperature of the OG was monitored using a metal sheath K-type thermocouple attached directly to one of its electrodes while thermal imaging camera (i3, Flir) was also used to monitor the silica glass tube temperature in case of the spiral-tubular OG assay.

Commercial surface DBD OG was electrically supplied using either its build-in HV power supply (~230 V mains-operated) or a laboratory variable sinusoidal HV supply system consisted of Agilent 33521a signal generator and Trek 20/20C HV amplifier. Only the latter laboratory HV supply set-up was used in case of the volume DBD OG of the spiral-tubular design. HV electric supply parameters were recorded using a digital oscilloscope (MSO2014, Tektronix) fitted with 1:1000 HV probe (HP 1137A) for HV (peak value) measurement and 1:10 probe (P1110, Tektronix) interfaced to 98.0 nF low loss capacitor connected in series with DBD OG for charge measurement.

All experimental data points presented if the figures were supplemented with dashed lines drawn to guide the eyes only, thus indicating no intended numerical data fit.

3. Results

3.1. Volume Spiro-Tubular DBD OG Design

The initial experiments involving the volume tubular DBD OG employing a brass internal axial HV electrode and a solid outer cylindrical Cu foil electrode were run at a low airflow rate (1.0 Nl/min). Figure 5a shows the recorded dependence of O_3 production on the 10 kV HV supply frequency. Increasing supply frequency steadily escalated O_3 throughput however, for a given airflow rate and the supply voltage, there was an optimal frequency of 700 Hz resulting in the maximized O_3 production reaching 3350 ppm_v. Further increase of the supply frequency resulted in the temperature rise bringing about O_3 concentration decline due to the predomination of O_3 thermal destruction over DBD ozone generation. The O_3 output was therefore mainly limited by the processed gas temperature, translated to the outer silica glass surface temperature of 40 °C in the optimal conditions for a given airflow rate, HV supply and internal electrode material.

Additional O_3 generation enhancement was achieved due to geometry-related management of DBDs and O_3-synthesis zones illustrated experimentally in Figure 5b for 1.0 Nl/min airflow and 10 kV sinusoidal HV supply. The spiral design of the outer GND electrode unambiguously enhanced O_3 throughput. By varying its width and pitch it was possible to increase the maximal O_3 concentration from 3550 ppm_v at the optimal 2.8 kHz and 7/32 mm width/pitch up to 3980 ppm_v at the optimal 1.2 kHz and 19/35 mm width/pitch. Thus, an almost 19% increase in O_3 production was attained at the cost of 71% supply power rise comparing to the solid Cu foil electrode (as the active supply power was directly proportional to the frequency). On the other hand, geometrical tweaking and supply power rise resulted in only a moderate increase of the overall process temperature, manifested in the silica glass tube temperature reaching 45 °C at the optimal O_3 yield conditions (Figure 5b).

Further ozone concentration enhancement was brought in by fitting the discussed volume DBD OG with an alumina-covered HV internal axial electrode. While such modification was introduced a steady production of 4180 ppm_v O_3 at 1 Nl/min airflow (corresponding to 0.54 g/h O_3) was commenced at optimized 10 kV 1.6 kHz sinusoidal HV supply and 19/35 mm outer spiral electrode, as illustrated in Figure 6a. O_3 production in such circumstances required 8.1 W of active supply power (as verified using measurement method based on voltage–charge *V-Q* Lissajous curve) and resulted in 0.09 W/cm^2

active power surface density translated into the maximal silica glass tube temperature of 46 °C and 67 g/kWh O_3 generation efficiency.
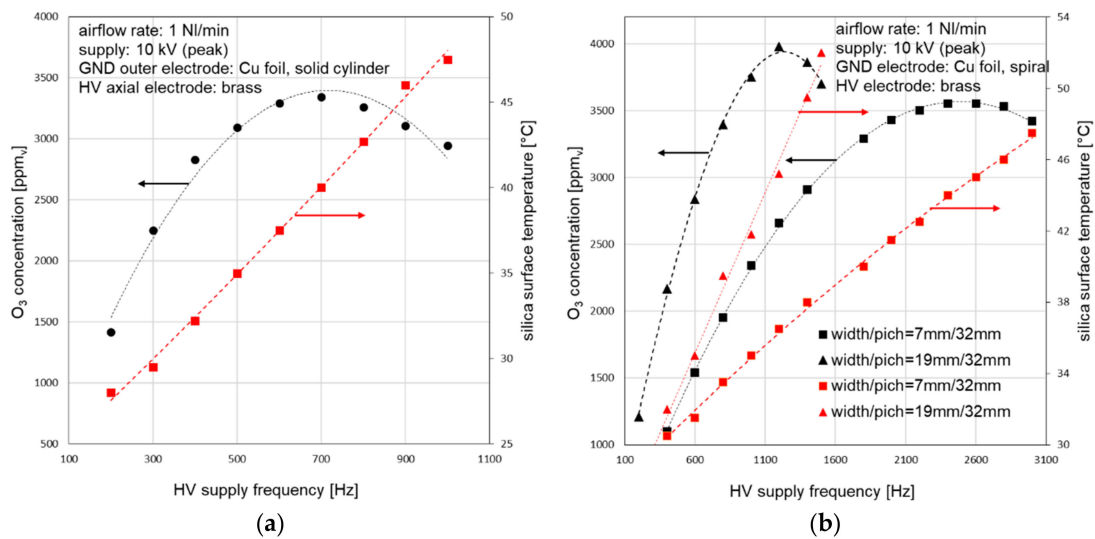

Figure 5. Variations of O_3 concentration and temperature in the volume DBD OG fitted with the internal brass electrode and outer Cu foil electrode of (**a**) solid design, (**b**) spiral design (supplied using variable-frequency 10 kV sinusoidal high voltage (HV) power supply at 1 Nl/min airflow).
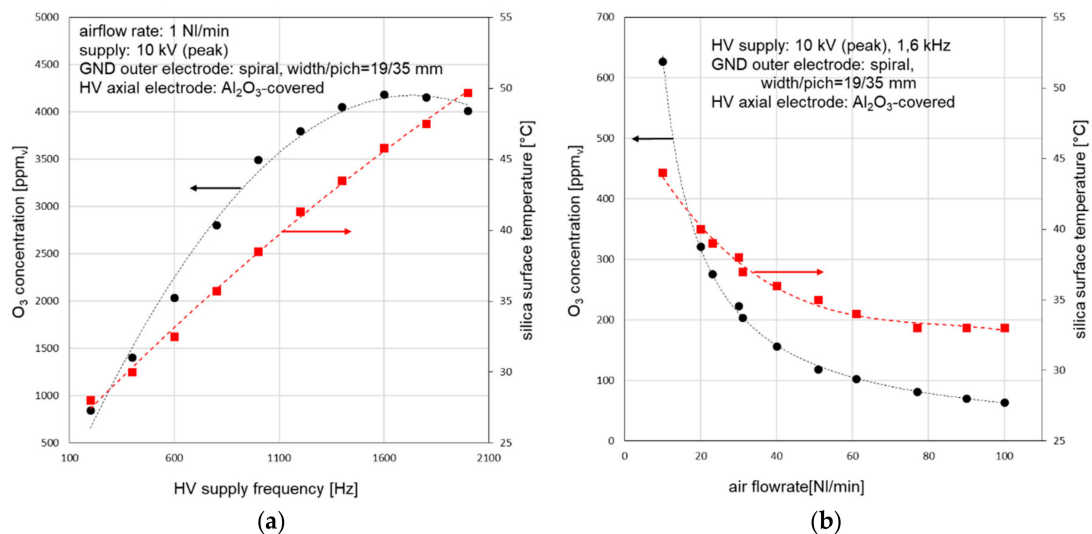

Figure 6. Variations of O_3 concentration and temperature in the volume DBD OG fitted with Al_2O_3-covered internal and 19/35mm width/pitch spiral outer Cu electrode supplied using 10 kV sinusoidal HV power supply: (**a**) at 1 Nl/min airflow, (**b**) at moderate airflow and 1.6 kHz HV power supply.

Experiments run at moderate airflow brought about even lower silica glass tube temperature which dropped to 33 °C at 100 Nl/min and 1.6 kHz 10 kV HV power supply (delivering 8.8 W active power at 0.1 W/cm^2 power surface density) as shown in Figure 6b. It such conditions production of O_3 decreased to 64 ppm$_v$ (corresponding to 0.82 g/h O_3 production and 93 g/kWh efficiency).

3.2. Surface DBD OG Design

In contrast to appealing experimental results presented so far for the volume DBD OG with a spiral electrode design, the examined commercial SDBD OG performed very feebly. Figure 7a

illustrates variations of O_3 concentration and electrode temperature recorded for the surface-type DBD OG two-plate unit supplied using its build-in mains-operated HV power supply at low air intake (1 Nl/min). Although the HV-supply energization triggered an abrupt rise of its O_3 output up to 2035 ppm$_v$, however, as the electrode temperature exceeded 29 °C, it started to decline and reached 12 ppm$_v$ at 48 °C and finally no O_3 was produced when temperature of the OG electrodes exceeded 90 °C after just 120 s of its operation. Thus, the commercial surface DBD OG design produced expedient amounts of O_3 at low airflow only when the temperature of its composite plates was below 48 °C but, on the other hand, if it was running on the build-in HV power supply longer than approximately 1 min generation of O_3 was completely brought to a standstill. At moderate air flowrate (as illustrated in Figure 7b) O_3 generation became unremitting. Its concentration remained very low (5–6 ppm$_v$) up to 25 Nl/min and then over 30 Nl/min escalated up to 59 ppm$_v$ observed at 100 Nl/min. It corresponded to 0.76 g/h of O_3 throughput at 100 Nl/min flow rate, which was over 10 times lower than the value quoted by the SDBD OG manufacturer.
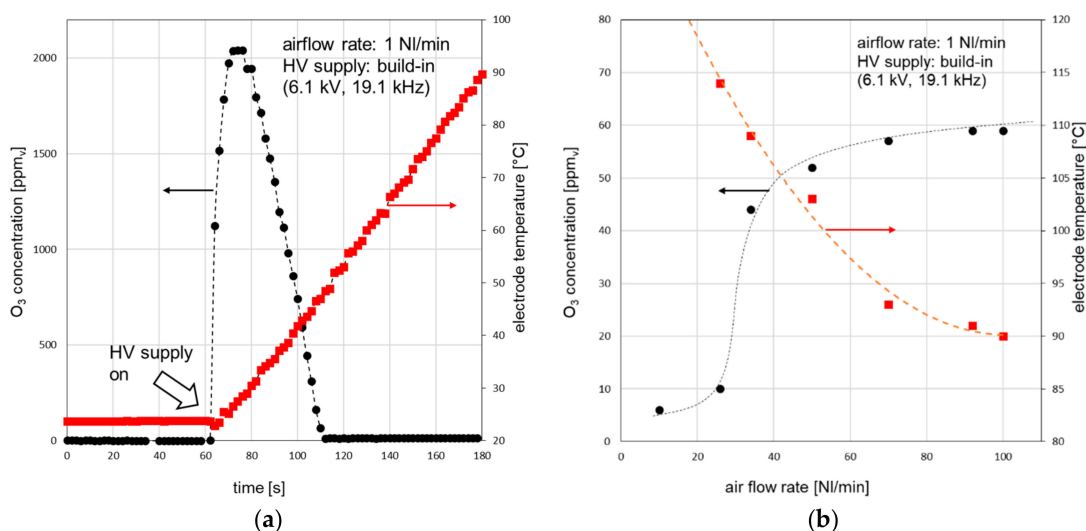

Figure 7. Variations of O_3 concentration and electrode temperature in surface DBD OG supplied using the build-in mains HV power supply at (**a**) 1 Nl/min air flow rate, (**b**) at moderate airflow.

Although elevated airflow rate facilitated cooling of the SDBD OG plates, even at 100 Nl/min their temperature exceeded 90 °C. Thus, even running the commercial SDBD OG at a high airflow rate, which was actually endorsed by its manufacturer, did not help in attaining the manufacturer-certified O_3 production. The observed swift rise of the SDBD OG temperature and its excessive final value was related to dense surface discharges sliding on its alumina exposed surface (Figure 8a) and to excessively high active supply power furnished by the original mains-operated HV supply (operating at 6.2–6.5 kV 19.1 kHz distorted sinusoidal voltage and delivering from 90 to 113 W).

Conversely, the ill-performing commercial SDBD OG was made to steadily produce 1115 ppm$_v$ O_3 at 1 Nl/min airflow (corresponding to 0.14 g/h O_3) when energized using purely sinusoidal HV supply at optimized 6.0 kV 1.1 kHz. Active power consumption of the SDBD OG in such a supply regime reached merely 7.4 W, which was equivalent to 18.9 g/kWh O_3 yield. In such a supply regime, O_3 generation was optimal when the temperature of the SDBD plates was kept below 50 °C. Although similar experiments run at moderate airflow rates, illustrated in Figure 8b, led to further reduction of the DBD plate temperature down to 30 °C at 100 Nl/min airflow yet the O_3 concentration plummeted in this conditions to 29 ppm$_v$, corresponding to 0.37 g/h.
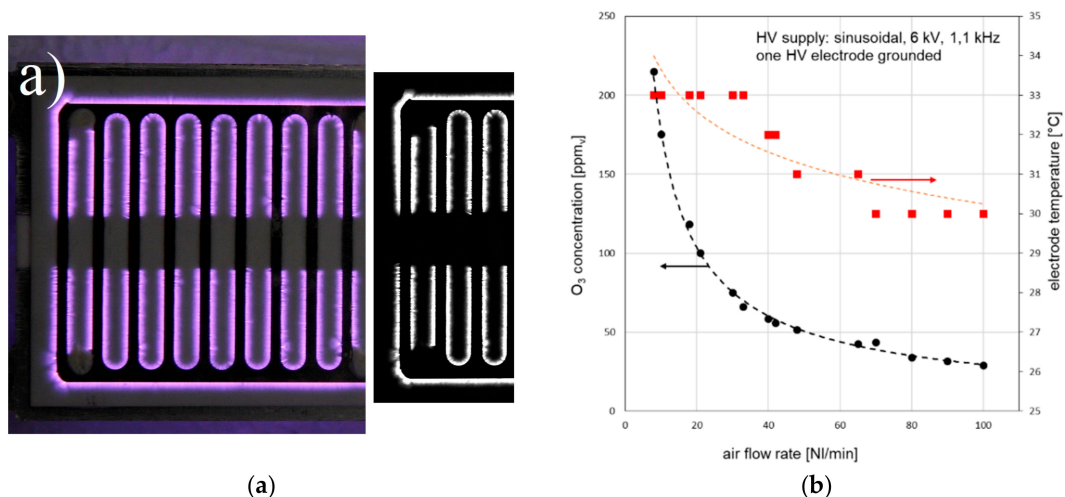
Figure 8. Surface DBD OG: (**a**) discharge pattern (real image and its digitally-processed section used for real discharge area calculation), (**b**) variations of O_3 concentration and electrode temperature at moderate airflow and optimized sinusoidal 6 kV 1.1 kHz HV power supply.

4. Discussion

The stability of gaseous O_3 is strongly temperature-, gas velocity- and humidity-dependent as its half-life time is reduced from approximately 1500 min (at 24 °C, 0% RH and no gas movement) to approximately 800 min at 40 °C, to approximately 700 min at 45% RH and to approximately 210 min at 100 m^3/h gas streaming [22]. Thus, if the relative humidity of the supply air is not varied significantly, correct thermal management of the OG operated at low gas velocity is mandatory when its optimal performance is targeted. As it was experimentally shown, tweaking the HV supply enabled effective thermal control of the volume DBD OG and its performance optimization. However, its extent was limited by self-cooling of the volume OG as no forced cooling was intended to be put into operation in the tested design.

The spiral design of the outer GND electrode enhanced O_3 throughput. First of all, spiral electrode geometry resulted in boosting O_3 production by keeping the process temperature at a moderate level at increased power supply conditions due to decreased volume in which discharge-generated heat transfer was commenced. However, it has also created recurring discharge-reach and discharge-free zones. Even narrowed discharge regions provided effective O_2 dissociation into excited O* atoms due to the fast nature (ns time scale) of electron and ion collision ionization processes. When conveyed to the discharge-free zones, O* atoms were effectively recombining with O_2 to form O_3 and this process was not interfered with by the discharges. A high density of discharges and thus generation of excessively energetic and concentrated excited species is known to lead to unfavorable recombination of O* into diatomic O_2 (resulting in no O_3 production) as well as to the reaction of O_3 with O* and electron-triggered dissociation of O_3 leading to the destruction of already formed O_3. According to Kitayama and Kuzumoto, the dissociation rate of O_3 is 6–8 times higher than the dissociation rate of O_2 molecule in the discharge channel [23]. Moreover, as the spiral design of the electrode system resulted in a subsided volume in which DBD non-thermal plasma was ignited, it may be accounted for diminished generation of atomic nitrogen N* (originating from electron impact dissociation of N_2). Thus, less NO and NO_2 nitrous oxides would be formed and therefore so-called autocatalytic cycle for O_3 destruction [24] would be less sizable (however such stipulation has not been verified experimentally in the presented research).

All those detrimental processes are electron energy- and temperature-amplified and decrease the overall effectiveness of O_3 formation. Thus, the geometrical introduction of discharge-free zones (supplying no energy to electrons and ions and providing moderate temperature) but still reach in the active oxygen atoms favored global O_3 synthesis effectiveness. To address the above remarks,

electrostatic and conjugated heat transfer finite element method (FEM) simulations were performed using the *Comsol Multiphysics* software package. The volume DBD OG design (with optimized 19/35mm spiral electrode width/pitch) was simplified by representing the outer helical electrode as 5 rings of the same total surface area separated by 16 mm distance (thus furnishing the same surface power density and similar heating and cooling conditions) while other dimensions of the model were kept analogous to the real design. Figure 9a illustrates simulated static electric field distribution in the volume DBD OG axisymmetric cross-section constrained to one of the outer electrode segments at the maximal 10 kV supply voltage. In order to better visualize the DBD region, Figure 9b expands the inter-electrode area in which the electric field was shown only in the region where the air breakdown strength of 4.37 MV/m was surpassed (as calculated for 1 mm discharge gap and 1 atm pressure according to Hussain and Nema [25]). As might be expected, the DBD region was limited merely to the ring-like sub-volume of the flow-through tubular gas channel zoned by the outer foil electrode.
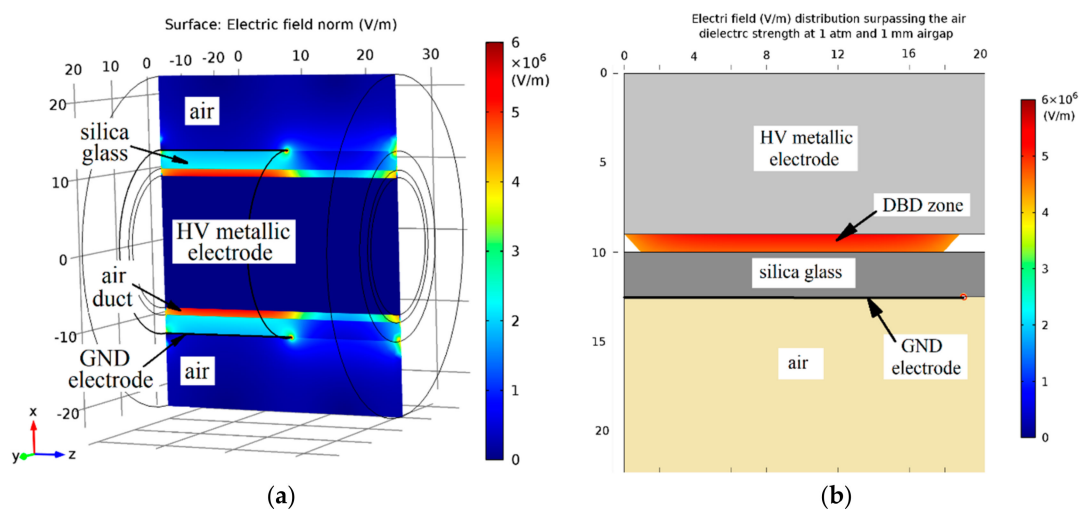

(a)　　　　　　　　　　　　　　　　　　　　　　　　　　　　　(b)

Figure 9. Electrostatic finite element method (FEM) simulation results for a simplified volume DBD OG model: (**a**) electric field distribution at 10 kV HV supply, (**b**) air gap breakdown section corresponding to Paschen air breakdown strength at 1 atm and 1 mm gap (spatial dimensions in mm).

For the purpose of the conjugated heat transfer FEM simulation, it was stipulated that only those inter-electrode ring narrow gas volumes were the sources of the heat generated by DBD and that the entire active supply energy was converted into heat in those volumes. Simulation results obtained for such a simplified model were shown in Figure 10a for the case of 1 Nl/min laminar airflow and 8.1 W active supply power. The simulated temperature of the outer silica surface was generally lower than that registered experimentally; 45 °C was modeled in the locations in the middle between the last two ring electrodes (at the point marked with X in Figure 10a) while 46 °C was observed experimentally in the corresponding location in the middle between the last twist of the real helical electrode. Similarly, underestimated temperature data was obtained when the simulation was run at 100 Nl/min air flow rate yielding 29 °C (as shown in Figure 10b) while 33 °C was registered empirically. The negative temperature bias discovered in both simulation cases might be related to the overestimated natural cooling modeled by the mean heat transfer coefficient (3.5 W/m^2 K) of the outer silica glass and copper electrode surface as well as to their overrated radiative cooling. The turbulent airflow conditions (which exist in the real tubular pneumatic system at 100 Nl/min air flow rate) have also not been taken into account in the FEM simulation.
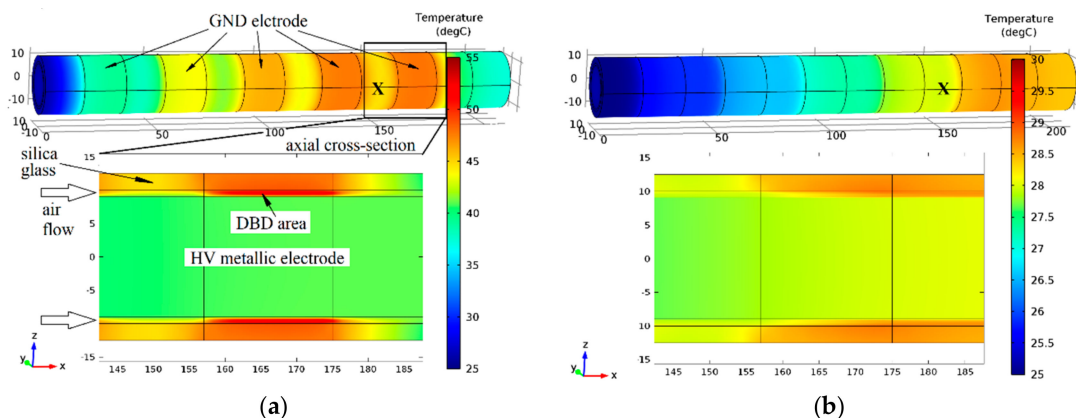
Figure 10. Thermal FEM simulation results for a simplified volume DBD OG model: (**a**) temperature distribution for 1 Nl/min airflow and 8.1 W active power supply, (**b**) for 100 Nl/min and 8.8 W (all spatial dimensions in mm).

There are literature references related to catalytic effects of Al_2O_3 in DBD ozone synthesis, however, such effects are pronounced in packed-bed-type ozonizers or if surface discharges are employed [26,27]. However, as it was verified experimentally a perceptible catalytic action of Al_2O_3 was also perceived in the presented volume-type DBD OG, accounting for approximately 5% increase in its performance in relation to the non-catalytic scheme using a brass internal electrode. As the optimal process temperature (manifested by the silica tube temperature) was almost identical in both cases (brass- and alumina-covered electrode) thus it seems to be justified that Al_2O_3 surface catalytic action was not temperature-activated in this low-temperature region.

On the other hand, the operation of a popular commercial SDBD OG was mostly bringing about thermal destruction of O_3. Very high active power consumption as well as the vigorous surface discharges advancing on the alumina plate exterior were responsible for the observed excessive thermal effects. Taking into account the estimated surface area covered by surface discharges (approximately 2.7 cm^2; calculated using digitally processed discharge image shown in Figure 5a inset) it was translated to 33–42 W/cm^2 active power density (a value comparable to power density used in electrical resistive water heaters [28]) and thus low O_3 generation efficiency of 8.4 g/kWh.

5. Conclusions

The presented spiral-electrode volume DBD OG operated at active power surface density 0.09–0.1 W/cm^2 achieved 67 g/kWh O_3 generation efficiency at low airflow rate (1 Nl/min) while at high airflow (100 Nl/min) its efficiency crested at 93 g/kWh. Those experimentally determined values are higher than figures of merit cited in the literature for photocatalytic DBD ozone generator designs and similar airflow rates [16,29]. However, as the obtained results are still 2–4 times lower than the maximal efficiency predicted by theoretical calculations (200–280 g/kWh, depending on the estimating methodology summarized in [30]) further optimization is still possible through research involving other photocatalyst selection as well as HV impulse supply.

Surprisingly, a commercially popular SDBD ozone generator, habitually yet incorrectly so-called "corona ozone generator" performed very feebly and proved to be very energy-ineffective and far from the manufacturer-stated ozone output yield due to its high operational temperature.

Conflicts of Interest: The author declares no conflict of interest.

References

1. Remondino, M.; Valdenassi, L. Different Uses of Ozone: Environmental and Corporate Sustainability. Literature Review and Case Study. *Sustainability* **2018**, *10*, 4783. [CrossRef]
2. Elvis, A.M.; Ekta, J.S. Ozone therapy: A clinical review. *J. Nat. Sci. Biol. Med.* **2011**, *2*, 66–70. [CrossRef] [PubMed]
3. Nath, A.; Mukhim, K.; Swer, T.; Dutta, D.; Verma, N.; Deka, B.C.; Gangwar, B. A Review on Application of Ozone in the Food Processing and Packaging. *J. Food Prod. Dev. Packag.* **2014**, *1*, 7–21.
4. Czapka, T.; Mirkowska, A.; Palewicz, M. Decolorization of methylene blue in aqueous medium using dielectric barrier discharge plasma reactor. *Prz. Elektrotechniczn.* **2017**, *93*, 188–191. [CrossRef]
5. National Institute for Occupational Safety and Health. NIOSH Pocket Guide to Chemical Hazards (3rd Printing with Minor Technical Revisions). Available online: http://www.cdc.gov/niosh/npg (accessed on 5 January 2020).
6. Ozone. Available online: https://pubchem.ncbi.nlm.nih.gov/compound/ozone (accessed on 10 May 2019).
7. Pekarek, S. Non-Thermal Plasma Ozone Generation. *Acta Polytech.* **2003**, *43*, 47–51.
8. Chang, J.-S.; Lawless, P.A.; Yamamoto, T. Corona Discharge Processes. *IEEE Trans. Plasma Sci.* **1991**, *19*, 1152–1166. [CrossRef]
9. Kuechler, A. *High Voltage Engineering Fundamentals–Technology–Applications*; Springer-Verlag: Berlin, Germany, 2018. [CrossRef]
10. Pekarek, S. DC corona discharge ozone production enhanced by magnetic field. *Eur. Phys. J. D* **2010**, *56*, 91–98. [CrossRef]
11. Zylka, P. *Surface Charge Evolution in Gaseous Voids: Ferroelectret Charging Model*; Wroclaw University of Science and Technology: Wroclaw, Poland, 2016; Unpublished manuscript.
12. Kogelschatz, U. Dielectric-barrier Discharges Their History, Discharge Physics, and Industrial Applications. *Plasma Chem. Plasma Process.* **2003**, *23*, 1–46. [CrossRef]
13. Kogelschatz, U.; Eliasson, B.; Egli, W. Dielectric-Barrier Discharges. Principle and Applications. *J. Phys. IV France* **1997**, *7*, 47–66. [CrossRef]
14. Mizuno, A. Recent Progress and Applications of Non-Thermal Plasma. *Int. J. Plasma Environ. Sci. Technol.* **2009**, *3*, 1–7.
15. Shohet, J.L. *Encyclopedia of Plasma Technology—Two Volume Set*; CRC Press: Boca Raton, FL, USA, 2016; ISBN 9781351204958.
16. Pekarek, S. Experimental study of surface dielectric barrier discharge in air and its ozone production. *J. Phys. D Appl. Phys.* **2012**, *45*, 075201. [CrossRef]
17. Siemens, W. Ueber die elektrostatische Induction und die Verzögerung des Stroms in Flaschendrähten. *Poggendorff's Annal. Phys. Chem.* **1857**, *178*, 66–122. [CrossRef]
18. Nasser, S.; Morris, S.; James, S. A Novel Fuel Efficient and Emission Abatement Technique for Internal Combustion Engines. *SAE Trans. J. Fuel Lubr.* **1998**, *107*, 1410–1425. [CrossRef]
19. Nishida, H.; Tachibana, T. Homogeneous Charge Compression Ignition of Natural Gas/Air Mixture with Ozone Addition. *J. Propul. Power* **2006**, *22*, 151–157. [CrossRef]
20. Wilk, M.; Magdziarz, A. Ozone Effects on the Emissions of Pollutants Coming from Natural Gas Combustion. *Pol. J. Environ. Stud.* **2010**, *19*, 1331–1336.
21. *Ozone: Different "Concentrations"*; Tech Note TN-2, rev. 4/2013; BMT Messtechnik GMBH: Stahnsdorf, Germany, 2013.
22. McClurkin, J.D.; Maier, D.; Ileleji, K.E. Half-life time of ozone as a function of air movement and conditions in a sealed container. *J. Stored Prod. Res.* **2013**, *55*, 41–47. [CrossRef]
23. Kitayama, J.; Kuzumoto, M. Theoretical and experimental study on ozone generation characteristics of an oxygen-fed ozone generator in silent discharge. *J. Phys. D Appl. Phys.* **1997**, *30*, 2453–2461. [CrossRef]
24. Yagi, S.; Tanaka, M. Mechanism of ozone generation in air-fed ozonisers. *J. Phys. D Appl. Phys.* **1979**, *12*, 1509–1520. [CrossRef]
25. Husain, E.; Nema, R.S. Analysis of Paschen curves for air, N_2 and SF_6 using the Townsend breakdown equation. *IEEE Trans. Dielect. Electr. Insul.* **1982**, *17*, 350–353. [CrossRef]
26. Huang, W.; Ren, T.; Xia, W. Ozone Generation by Hybrid Discharge Combined with Catalysis. *Ozone Sci. Eng.* **2007**, *29*, 107–112. [CrossRef]

27. Chen, H.L.; Lee, H.M.; Chang, M.B. Enhancement of Energy Yield for Ozone Production via Packed-Bed Reactors. *Ozone Sci. Eng.* **2006**, *28*, 111–118. [CrossRef]

28. Chromalox Technical Information: Allowable Watt Density & Heater Selection–Guidelines. Available online: http://www.chromalox.com/catalog/resources/technical-information/Heat-Loss-Calculations-and-Heater-Selection-Watt-Density.pdf (accessed on 13 January 2020).

29. Pekarek, S.; Usama, K. Ozone generation by surface dielectric barrier discharge with TiO_2 photocatalyst. In Proceedings of the 30th International Conference on Phenomena in Ionized Gases ICPIG, Belfast, Northern Ireland, UK, 28 August–2 September 2011.

30. Plank, T.; Jalakas, A.; Aints, M.; Paris, P.; Valk, F.; Viidebaum, M.; Jõgi, I. Ozone generation efficiency as a function of electric field strength in air. *J. Phys. D Appl. Phys.* **2014**, *47*, 335205. [CrossRef]